Tuning topological surface magnetism by bulk alloying

N. Klier,[1] S. Sharma,[2] F. Rost,[1] O. Pankratov,[1,*] and S. Shallcross[1,†]
[1]*Lehrstuhl für Theoretische Festkörperphysik, Staudtstrasse 7-B2, 91058 Erlangen, Germany,*
[2]*Max-Planck-Institut für Mikrostrukturphysik, Weinberg 2, 06120 Halle, Germany*

(Received 26 April 2018; published 15 August 2019)

Deploying an analytical atomistic model of the bulk band structure of the IV-VI crystalline topological insulators, we connect the spin structure of the surface state to the crystal field and spin-orbit coupling parameters of the bulk material. While the Dirac-Weyl-type topological surface state is often assumed to be universal, we show that the physics of the surface state is strikingly nonuniversal, carrying a profound imprint of the bulk physics. To see this explicitly we calculate the Ruderman-Kittel-Kasuya-Yosida interaction, which may be viewed as a probe of this surface state spin structure, finding that its *qualitative form* depends on the values the bulk spin-orbit and crystal field parameters take. This opens the way to tune the spin interaction on the surface of a IV-VI topological insulator by, for instance, varying the composition of the IV-VI ternary compounds.

DOI: 10.1103/PhysRevB.100.075130

I. INTRODUCTION

The Ruderman-Kittel-Kasuya-Yosida (RKKY) interaction is an indirect exchange interaction of external spins mediated by the virtual excitations of an electron gas [1–4]. While the RKKY interaction is strongly suppressed in insulators due to the bulk band gap, this changes dramatically in topological insulators that feature inherent metallic surface states. These surface states are spin polarized and reflect the nontrivial topology of the bulk electronic structure, physics that will also be encoded in the RKKY interaction. However, for most topological insulators, which are rather complex materials, it is practically impossible to provide in analytical form the connection between the bulk and the surface topological states and hence to understand the surface RKKY coupling in terms of the bulk electronic structure.

As a consequence, the RKKY interaction in topological insulators has, to date, been addressed on the basis of *generic* Dirac-Weyl Hamiltonians [5–14]. These investigations have uncovered a rich RKKY physics in the topological surface state which features a wide variety of coupling interactions: Ising, Heisenberg, and Dzyaloshinskii-Moriya, which can also be found in Weyl metals [15,16]. Such an approach, however, excludes the possibility of analyzing the relation between the bulk electronic structure and the surface RKKY interaction. In particular, interesting questions such as how the rich RKKY behavior of topological insulators might be tuned by manipulating the bulk physics, e.g., by alloying, cannot be answered. In this paper we remedy this situation by establishing an explicit link between bulk band gap states and the topological surface wave functions for the IV-VI crystalline topological insulators [17–28] and on this basis analyze the impact of bulk physics on the RKKY interaction.

We find that despite the universal form of the Dirac-Weyl topological surface state the spin structure, as probed by the RKKY interaction, is strikingly nonuniversal and depends qualitatively on the spin mixing of the bulk band edge states that, in turn, depend on the crystal field environment and spin-orbit coupling in the bulk. Note that while the envelope of the RKKY interaction is obviously universal, the spin function prefactor of the RKKY [i.e., Ising $S_i^z S_j^2$, Heisenberg $\mathbf{S}_i.\mathbf{S}_j$, or Dzyaloshinskii-Moriya $(\mathbf{S}_i \times \mathbf{S}_j) \cdot \hat{\mathbf{z}}$] is not and reflects the physics of local scattering from spin impurities in the electron gas. It is this that allows us to employ the RKKY interaction as a probe of the surface spin structure, and it is the relative weight of these distinct spin functions in the overall RKKY interaction that is sensitive to bulk physics. As a specific example, we show that for the well-known SnTe topological insulator the form of the RKKY interaction can be strongly influenced by alloying with Pb in the bulk, with, at ∼60 Å of separation, the equilibrium spin configuration switching from parallel to perpendicular to the vector connecting the spin impurities.

II. THE BULK BAND STRUCTURE MODEL FOR THE IV-VI COMPOUNDS

The IV-VI materials crystallize in a cubic NaCl-type lattice with six p bands around the Fermi energy (three conduction and three valence bands) that originate from the atomic p shells of the group IV and group VI species. The low-energy sector is at the high-symmetry L point at which, as shown in Refs. [17,18], the wave function parity provides a good quantum number. The Bloch functions at the L point are therefore of pure group IV and group VI character. In what follows our coordinate system is chosen such that the group-IV-derived Bloch states have odd parity and the group-VI-derived Bloch states have even parity. While the admixture of the atomic s states can be considerable, it does not change the *form* of the effective Hamiltonian and thus can be included by tuning the value of the model parameters to fit band structure calculated *ab initio*.

In the absence of interaction between these Bloch states, two atomic p states would give rise to two degenerate triplets

*oleg.pankratov@fau.de
†sam.shallcross@fau.de

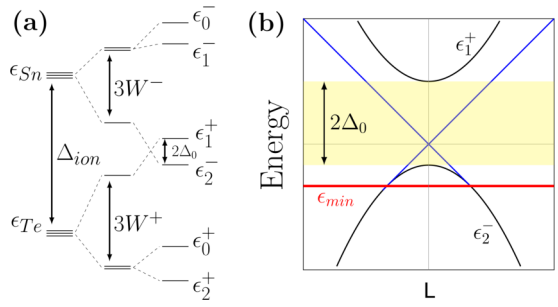

FIG. 1. (a) Schematic illustration of the band ordering at the L point showing the band inversion that occurs in SnTe due to crystal field and spin-orbit coupling effects. Without crystal field and spin orbit the p orbitals at the L point are threefold degenerate, separated in energy only by the difference in ionization energy between the group IV and group VI species; crystal field splitting by $3W^{\pm}$ lifts this to a $2+1$ degeneracy, which is then completely lifted by the spin-orbit interaction. For sufficiently large crystal field and spin orbit, the ordering of the Sn and Te states is interchanged, leading to a nontrivial topological surface state. (b) The low-energy band structure in the vicinity of the L points, exhibiting the two linear surface bands (blue) that meet tangentially with the lower bulk band (black) at the energy $\epsilon_{\min}$. The gap $2\Delta_0$ is illustrated by the shaded region.

of cubically symmetric bands at the L points, ordered such that the triplet of odd-parity $(-)$ group IV states is higher in energy than the triplet of even-parity $(+)$ group VI states. This is shown in Fig. 1(a). This degeneracy is, however, lifted by the crystal field effect (which mixes p orbitals) and results in $2+1$ p levels separated by the crystal field matrix element $W^{\pm}$ and the spin-orbit coupling $\lambda^{\pm}$ (which mixes spin channels) and finally completely lifts the original threefold degeneracy. These two stages are shown in the schematic illustration presented in Fig. 1(a). In the case of SnTe or cubic SnSe this breaking up of the p-level degeneracy is sufficient to invert the ordering of the ϵ_1^+ and ϵ_2^- states compared to the vacuum, as illustrated in Fig. 1(a), resulting in a topologically protected surface state.

The Bloch states at the L points are given in terms of p orbitals $p_{x,y,z}(\mathbf{r})$ by

$$\Phi^+_{x,y,z}(\mathbf{r}) = i\sqrt{\frac{2}{N}}\sum_{\mathbf{R}} \sin(\mathbf{k}_L\mathbf{R})p_{x,y,z}(\mathbf{r}-\mathbf{R}), \tag{1}$$

$$\Phi^-_{x,y,z}(\mathbf{r}) = \sqrt{\frac{2}{N}}\sum_{\mathbf{R}} \cos(\mathbf{k}_L\mathbf{R})p_{x,y,z}(\mathbf{r}-\mathbf{R}), \tag{2}$$

where $\mathbf{k}_L = \pi/a(1,1,1)$ is one of the eight L-point wave vectors and $\mathbf{R}$ runs over all lattice vectors. As a result of spin and orbital angular momentum mixing described above and illustrated in Fig. 1(a), the band edge states at the L point are given by the Kramers conjugate pairs,

$$\Phi_2^- = -\sin\left(\frac{\theta_-}{2}\right)\Phi_+^{-\downarrow} + \cos\left(\frac{\theta_-}{2}\right)\Phi_0^{-\uparrow}, \tag{3}$$

$$K\Phi_2^- = -\sin\left(\frac{\theta_-}{2}\right)\Phi_-^{-\uparrow} + \cos\left(\frac{\theta_-}{2}\right)\Phi_0^{-\downarrow}, \tag{4}$$

$$\Phi_1^+ = \cos\left(\frac{\theta_+}{2}\right)\Phi_+^{+\downarrow} + \sin\left(\frac{\theta_+}{2}\right)\Phi_0^{+\uparrow}, \tag{5}$$

$$K\Phi_1^+ = \cos\left(\frac{\theta_+}{2}\right)\Phi_-^{+\uparrow} + \sin\left(\frac{\theta_+}{2}\right)\Phi_0^{+\downarrow}, \tag{6}$$

where K is the Kramers conjugate operator, $\Phi_0^{\pm\uparrow\downarrow} = \Phi_z^{\pm\uparrow\downarrow}$, $\Phi_{\pm}^{\pm\uparrow\downarrow} = 1/\sqrt{2}(\Phi_x^{\pm\uparrow\downarrow} \pm i\Phi_y^{\pm\uparrow\downarrow})$, and the coordinate system has the z axis aligned along the (111) symmetry axis which forms a natural coordinate system. The *spin-mixing parameters* $\theta_{\pm}$ are connected to the matrix elements of crystal field $W^{\pm}$ and the spin-orbit interaction $\lambda^{\pm}$ as follows [18]:

$$\tan\theta_{\pm} = -\frac{2\sqrt{2}\hbar\lambda^{\pm}}{\hbar\lambda^{\pm} + 3W^{\pm}}. \tag{7}$$

This parameter will subsequently be shown to dramatically influence the RKKY interaction on the (111) surface of these materials. As shown in Ref. [18], the C_{3v} symmetry of the L point dictates the following Hamiltonian:

$$H^{\pm} = \mp\Delta_{ion} + 2W^{\pm}\cos\left(\frac{2\pi}{3}L_z\right) + \lambda^{\pm}(\mathbf{L}\cdot\boldsymbol{\sigma})^{\pm}, \tag{8}$$

where the $\pm$ index refers to the conduction band edge (group-VI-derived even-parity state) or the valence band edge (group-IV-derived odd-parity state) and where $\mathbf{L}$ is the angular momentum operator. The first term in Eq. (8) represents the difference in ionization energy between the group IV and group VI species; the second term encodes the mixing of the p orbitals, which, in the Hilbert space of the three p states, is equivalent to the actions of the rotation operator by angles of $2\pi/3$ around the (111) symmetry axis. The third term is the spin-orbit coupling. The parameters $W^{\pm}$ and $\lambda^{\pm}$ are tabulated in Refs. [17,18] for all IV-VI compounds. Finally, a $\mathbf{k}\cdot\mathbf{p}$ expansion around the L point leads to a 12-band $\mathbf{k}\cdot\mathbf{p}$ Hamiltonian, which reduces at low energies to a four-band Dirac-type Hamiltonian [18],

$$H = \begin{pmatrix} \Delta_0 & \hbar[v_\perp\boldsymbol{\sigma}_\perp\cdot\mathbf{k}_\perp + v_\parallel\sigma_z k_z] \\ \hbar[v_\perp\boldsymbol{\sigma}_\perp\cdot\mathbf{k}_\perp + v_\parallel\sigma_z k_z] & -\Delta_0 \end{pmatrix}, \tag{9}$$

where $\boldsymbol{\sigma}_\perp$ and $\mathbf{k}_\perp$ stand for the vectors of the Pauli matrices (σ_x,σ_y) and (k_x,k_y), respectively. In addition to the bulk band gap Δ_0, the Hamiltonian contains the velocities parallel and perpendicular to the (111) symmetry axis, $v_\parallel$ and $v_\perp$, respectively. These velocities encode the anisotropic effective masses parallel or perpendicular to this axis, responsible for the ellipsoidal deformation of constant-energy surfaces about the (111) symmetry axis. Most important, however, is that the basis functions of Eq. (9) are the L-point band edge wave functions (3)–(6).

III. THE TOPOLOGICAL SURFACE STATES

To describe the low-energy electron excitations on the surface at $z=0$ we take Eq. (9) and replace the band gap Δ_0 by a *band gap function* $\Delta(z) = \Delta_0 f(z)$ such that $\Delta(z\to-\infty)\to\Delta_0$, the bulk value of the band gap, and $\Delta(z\to+\infty)\to\infty$ to mimic the vacuum state. We thus require the function $f(z)$ to satisfy $f(-\infty)\to 1$ and $f(\infty)\to\infty$. For a topologically

nontrivial solution we further require gap inversion in the bulk, i.e., $\Delta_0 < 0$ [19]. Finally, we introduce an energy shift function $\varphi(z) = \varphi_0 f(z)$ that models the expected overall shift in energy of the states at the surface [20] (i.e., band bending). This yields the bulk-boundary eigenvalue problem

$$\begin{pmatrix} \Delta(z) & \hbar[v_\parallel \sigma_z k_z + v_\perp \boldsymbol{\sigma}_\perp \cdot \mathbf{k}_\perp] \\ \hbar[v_\parallel \sigma_z k_z + v_\perp \boldsymbol{\sigma}_\perp \cdot \mathbf{k}_\perp] & -\Delta(z) \end{pmatrix} \psi = [\epsilon - \varphi(z)]\psi. \tag{10}$$

Note that the definition used here of $f(z)$ implies that downward band bending is associated with positive φ_0 and upward band bending is associated with negative φ_0. There are four inequivalent L points in the bulk with, for the (111) surface, $\pi/a(1,1,1)$ projecting to the Γ point of the (111) surface Brillouin zone and $\pi/a(-1,1,1)$, $\pi/a(1,-1,1)$, and $\pi/a(1,1,-1)$ projecting to the three inequivalent M points. For reasons that will be explained below we focus on the Γ point of the (111) surface. This choice is, in fact, already implied by Eq. (10): Setting up the bulk-boundary problem for another crystal facet—or an L point oblique to the (111) axis—would require rotation of k_z in Eq. (9), as the principle axis of the ellipsoidal band manifold would no longer coincide with the surface normal.

As shown in Ref. [29], after squaring and transformation by

$$Z = \begin{pmatrix} \sqrt{\varphi_0 - \Delta_0} & \sqrt{\varphi_0 - \Delta_0} \\ \sqrt{\varphi_0 + \Delta_0} & -\sqrt{\varphi_0 + \Delta_0} \end{pmatrix} \otimes \sigma_0, \tag{11}$$

Eq. (10) takes on the supersymmetric form [29]

$$a^\dagger a(Z^{-1}\psi) = \left[\epsilon^2 - \hbar^2 v_\perp^2 k_\perp^2 + \frac{\epsilon^2 \varphi_0^2}{\Delta_0^2 - \varphi_0^2}\right](Z^{-1}\psi), \tag{12}$$

where $a = [i\tau_z \otimes \sigma_z v_\parallel p_z - W(z)]$, with

$$W(z) = \sqrt{\Delta_0^2 - \varphi_0^2}\left[f(z) + \epsilon\varphi_0/\left(\Delta_0^2 - \varphi_0^2\right)\right] \tag{13}$$

being the superpotential. This equation has two obvious zero-mode solutions, given by $\zeta_+ = |\uparrow\rangle \otimes |\uparrow\rangle\, g(z)$ and $\zeta_- = |\downarrow\rangle \otimes |\downarrow\rangle\, g(z)$, where the envelope function $g(z) = N \exp[\frac{1}{\hbar v_\parallel}\int_0^z dz\ W(z)]$, with normalization constant N, and $|\sigma\rangle$ are the eigenfunctions of σ_z. For $g(z)$ to be normalizable, evidently, the superpotential must change sign asymptotically as $W(z \to +\infty) < 0$ and $W(z \to -\infty) > 0$, and this is ensured by our definition of $f(z)$ provided that $|\varphi_0| < |\Delta_0|$ (i.e., the energy shift function is lower in magnitude than the band gap). That $W(z)$ asymptotically changes sign further implies that the zero-mode solutions are bounded in energy: For the experimentally observed downward band bending [30] we find a minimum energy $\epsilon_{\min}$ given by

$$\epsilon_{\min} = -\varphi(-\infty)\left(\Delta_0^2/\varphi_0^2 - 1\right). \tag{14}$$

The two zero-mode solutions (12) may be used as a basis for the interface Dirac equation [Eq. (10)], which after straightforward manipulation takes on the form of an effective Dirac-Weyl equation,

$$\hbar\gamma v_\perp \boldsymbol{\eta}_\perp \cdot \mathbf{k}_\perp \chi = \epsilon\chi, \tag{15}$$

where $\boldsymbol{\eta}$ is a pseudospin vector (η_x, η_y) and $\gamma = \sqrt{1 - \varphi_0/\Delta_0}$. η_x and η_y are the usual Pauli matrices; the different symbol is employed here to emphasize that the pseudospin space of Eq. (15) is different from the bulk pseudospin variables as well as, crucially, physical spin: χ is a wave function in the zero-mode subspace, i.e., $\chi = \chi_+\zeta_+ + \chi_-\zeta_-$. This equation, as is well known, describes massless Dirac fermions, and the surface spectrum consists of two linear dispersing energy bands $\epsilon_{k_\perp l} = l\hbar\gamma v_\perp k_\perp$, where $k_\perp = \sqrt{k_x^2 + k_y^2}$, where $l = \pm 1$ labels the two bands. The corresponding eigenstates are given by

$$\chi_{\mathbf{k}_\perp l} = \frac{1}{\sqrt{2}}\begin{pmatrix} e^{-i\frac{\phi}{2}} \\ l e^{i\frac{\phi}{2}} \end{pmatrix} e^{i\mathbf{k}\cdot\mathbf{r}}, \tag{16}$$

where $\phi = \tan^{-1} k_y/k_x$. The lower energy bound for the existence of zero modes can now be realized as a continuum energy at which the surface mode joins the bulk spectrum. At this energy the Dirac cone tangentially meets the bulk valence bank, as shown in Fig. 1(b) for the case of downwards band bending.

This solution is, obviously, not the physical wave function of the surface state. We obtain this with a two-step process: (i) first, we back transform to find the surface state solution of the original Dirac interface equation, Eq. (9), $Z(\chi_+\zeta_+ + \chi_-\zeta_-)$, and, crucially, (ii) we then express this in terms of the bulk basis function states [Eqs. (3) to (6)] that are the physical basis functions of the Dirac interface equation. In this way we find that the effective surface Hamiltonian and its eigenstates are defined on a pseudospin space that is spanned by the Kramers conjugate pair X and KX with

$$X = \frac{1}{\sqrt{2}}\left[e^{-i\frac{\pi}{4}}\sqrt{1 - \frac{\varphi_0}{\Delta_0}}\Phi_2^- + e^{i\frac{\pi}{4}}\sqrt{1 + \frac{\varphi_0}{\Delta_0}}\Phi_1^+\right], \tag{17}$$

leading to the physical wave function of the surface state given by

$$\Psi_{\mathbf{k}_\perp l} = \left(e^{-i\frac{\phi}{2}}X + l e^{i\frac{\phi}{2}}KX\right)e^{i\mathbf{k}_\perp\cdot\mathbf{r}_\perp} g(z)/\sqrt{2}. \tag{18}$$

As our theory distinguishes in a clear way the physical electron spin from the pseudospin degree of freedom, we can calculate expectation values of both the pseudospin and electron spin operators from the same surface state $\chi_{\mathbf{k}_\perp l}$. For the pseudospin we find the usual irrotational pseudospin density vector field $\langle\Psi_{\mathbf{k}_\perp l}|\boldsymbol{\eta}|\ |\Psi_{\mathbf{k}_\perp l}\rangle = l(\cos\phi,\ \sin\phi,\ 0)$ *with unit magnitude*, while, in contrast, the physical spin density is the well-known solenoidal field $\langle\Psi_{\mathbf{k}_\perp l}|\hat{\mathbf{S}}/\hbar|\ |\Psi_{\mathbf{k}_\perp l}\rangle = ls(-\sin\phi,\ \cos\phi,\ 0)$, with a *variable magnitude* that depends explicitly on the bulk band structure parameters $s = 1/2\cos[(\theta_- + \theta_+)/2] - \varphi_0/(2\Delta_0)\cos[(\theta_- - \theta_+)/2]$. Note that as we have derived our surface state from a microscopic theory of the bulk crystal, the value of s incorporates the bulk spin-orbit coupling that is known to reduce the spin polarization of the surface state [31].

IV. THE RKKY INTERACTION

We now come to the RKKY interaction between two magnetic moments on the surface of a IV-VI topological insulator. We will consider the Γ-point Dirac cone on the (111) surface and ignore the possible contribution from the M-point cones.

This is likely to be a rather good approximation as the energy separation of the Γ- and M-point cones (≈170 meV), along with the limited energy range within which the Dirac cone exists (≈200 meV), implies that for energies at which the RKKY signal from the Γ cone is strong, that from the M cone will be weak.

We consider the indirect exchange interaction to be mediated by the topological surface states, Eq. (16), and assume that each impurity spin $\mathbf{S}_{1,2}$ couples via a contact interaction to the electron spin density $\mathbf{s}_{1,2}$,

$$V = -\lambda(\mathbf{S}_1 \cdot \hat{\mathbf{s}}_1 + \mathbf{S}_1 \cdot \hat{\mathbf{s}}_2), \tag{19}$$

where the coupling strength is given by λ. As a further simplification of the model we set the energy shift function $\varphi_0 = 0$ (i.e., no band bending at the surface), an approximation expected to be good provided the Fermi energy does not approach the tangent point of the Dirac cone at which the surface state merges with the bulk spectrum.

To calculate the RKKY interaction we begin with the one-loop interaction energy

$$E_\alpha^{\text{int}}(\mathbf{R}_\perp) = -\frac{1}{\pi}\left(\frac{\hbar\lambda}{2}\right)^2 \int_{-\infty}^{E_F} dE \,\text{Im}\{\text{Tr}[(\boldsymbol{\sigma}\cdot\mathbf{S}_1)_\alpha \times G^{0R}(-\mathbf{R}_\perp, E)(\boldsymbol{\sigma}\cdot\mathbf{S}_2)_\alpha G^{0R}(\mathbf{R}_\perp, E)]\}, \tag{20}$$

expressed in the basis of the topological surface states X and KX, where α takes the value -1 on the group-IV-terminated surface and $+1$ on the group-VI-terminated surface, with the impurity separation vector $\mathbf{R}_\perp$. The two ingredients for the spin-spin interaction are therefore the Green's function $G^{0R}(\mathbf{R}_\perp, E)$, describing propagation through the electron gas, and the scattering matrices $\boldsymbol{\sigma}\cdot\mathbf{S}_1$ and $\boldsymbol{\sigma}\cdot\mathbf{S}_2$, describing the local spin scattering physics. The real-space propagator is given by the Dirac-Weyl form

$$G^{0R}(\mathbf{R}_\perp, E) = -i\frac{\pi^2(E+i\eta)}{\hbar^2 v_\perp^2 \Omega_{SBZ}} \times \begin{pmatrix} H_0^1\left(\frac{(E+i\eta)}{\hbar v_\perp}R_\perp\right) & ie^{-i\theta}H_1^1\left(\frac{(E+i\eta)}{\hbar v_\perp}R_\perp\right) \\ ie^{i\theta}H_1^1\left(\frac{(E+i\eta)}{\hbar v_\perp}R_\perp\right) & H_0^1\left(\frac{(E+i\eta)}{\hbar v_\perp}R_\perp\right) \end{pmatrix}, \tag{21}$$

where $H_\nu^1(x)$ stands for the Hankel function of the first kind of order ν, Ω_{SBZ} stands for the area of the surface Brillouin zone, and we have expressed the impurity separation vector in polar coordinates, where it takes the radius $R_\perp$ and the polar angle θ. To derive the scattering matrices $\boldsymbol{\sigma}\cdot\mathbf{S}_1$ and $\boldsymbol{\sigma}\cdot\mathbf{S}_2$ we evidently need to write only the vector of Pauli matrices $\boldsymbol{\sigma} = (\sigma_x, \sigma_y, \sigma_z)$ in the group IV or group VI subspace. For scattering at a group IV site impurity the $\boldsymbol{\sigma}\cdot\mathbf{S}_1$ matrix then takes the form

$$(\hat{\mathbf{s}}_1\cdot\mathbf{S}_1)_- = \frac{\hbar}{2}\mathbf{S}_1\cdot\begin{pmatrix} \langle\Phi_2^-|\boldsymbol{\sigma}|\Phi_2^-\rangle & \langle\Phi_2^-|\boldsymbol{\sigma}|K\Phi_2^-\rangle \\ \langle K\Phi_2^-|\boldsymbol{\sigma}|\Phi_2^-\rangle & \langle K\Phi_2^-|\boldsymbol{\sigma}|K\Phi_2^-\rangle \end{pmatrix} = \frac{\hbar}{4}\begin{pmatrix} S_1^z\cos\theta_- & iS_1^-\cos^2\left(\frac{\theta_-}{2}\right) \\ -iS_1^+\cos^2\left(\frac{\theta_-}{2}\right) & -S_1^z\cos\theta_- \end{pmatrix}, \tag{22}$$

while for scattering at a group VI site impurity it is given by

$$(\hat{\mathbf{s}}_1\cdot\mathbf{S}_1)_+ = \frac{\hbar}{2}\mathbf{S}_1\cdot\begin{pmatrix} \langle\Phi_1^+|\boldsymbol{\sigma}|\Phi_1^+\rangle & \langle\Phi_1^+|\boldsymbol{\sigma}|K\Phi_1^+\rangle \\ \langle K\Phi_1^+|\boldsymbol{\sigma}|\Phi_1^+\rangle & \langle K\Phi_1^+|\boldsymbol{\sigma}|K\Phi_1^+\rangle \end{pmatrix} = \frac{\hbar}{4}\begin{pmatrix} -S_1^z\cos\theta_+ & -iS_1^-\sin^2\left(\frac{\theta_+}{2}\right) \\ iS_1^+\sin^2\left(\frac{\theta_+}{2}\right) & S_1^z\cos\theta_+ \end{pmatrix}, \tag{23}$$

with $S_1^\pm = S_1^x \pm iS_1^y$. Note that already in these spin scattering matrices we see the explicit dependence of the bulk spin structure through the dependence on the spin-mixing angles $\theta_\pm$. Substituting Eqs. (21), (22), and (23) into Eq. (20) then leads to the following interaction energy:

$$\frac{E_\alpha^{\text{int}}(R_\perp)}{\kappa} = [A_{k_F}(R_\perp) - B_{k_F}(R_\perp)]\left[a_\alpha S_1^x S_2^x + b_\alpha S_1^z S_2^z\right] + [C_{k_F}(R_\perp) + D_{k_F}(R_\perp)]c_\alpha\left[S_1^x S_2^z - S_1^z S_2^x\right] + [A_{k_F}(R_\perp) + B_{k_F}(R_\perp)]a_\alpha S_1^y S_2^y, \tag{24}$$

where the RKKY coupling strength is $\kappa = -\frac{2\pi^2\hbar\lambda^2}{\Omega_{SBZ}^2 v_\perp}$ and the material-dependent coefficients a_α, b_α, and c_α are given in Table I. The remaining constants are material independent and are given by the integrals

$$A_{k_F}(R_\perp) = \frac{\pi}{2}\lim_{s\to 0}\int_{k_F}^\infty dk_\perp\, k_\perp^2 J_0(k_\perp R_\perp)Y_0(k_\perp R_\perp)e^{-sk_\perp}, \tag{25}$$

$$B_{k_F}(R_\perp) = \frac{\pi}{2}\lim_{s\to 0}\int_{k_F}^\infty dk_\perp\, k_\perp^2 J_1(k_\perp R_\perp)Y_1(k_\perp R_\perp)e^{-sk_\perp}, \tag{26}$$

$$C_{k_F}(R_\perp) = \frac{\pi}{2}\lim_{s\to 0}\int_{k_F}^\infty dk_\perp\, k_\perp^2 J_1(k_\perp R_\perp)Y_0(k_\perp R_\perp)e^{-sk_\perp}, \tag{27}$$

$$D_{k_F}(R_\perp) = \frac{\pi}{2}\lim_{s\to 0}\int_{k_F}^\infty dk_\perp\, k_\perp^2 J_0(k_\perp R_\perp)Y_1(k_\perp R_\perp)e^{-sk_\perp}, \tag{28}$$

with $k_\perp = E/(\hbar v_\perp)$, where J and Y are Bessel functions of the first and second kind, respectively. Following an asymptotic expansion by making the substitution $x = ER_\perp/(\hbar v_\perp)$ and replacing the Bessel functions by their asymptotics for large

TABLE I. The coefficients for the RKKY interaction on the surface of a topological insulator of the SnTe class: a_α is the in-plane Ising coupling, b_α is the out-of-plane Ising coupling, and v_α is the Dzyaloshinskii-Moriya coupling. The spin-mixing parameter θ_α is for the range of IV-VI semiconductors given in Ref. [18]. The parameter α takes the value -1 for the group-IV-terminated surface and $+1$ for the group-VI-terminated surface. These parameters are plotted in Fig. 2.

Coefficient	Value
a_α	$\frac{1}{4}\cos^4\left(\frac{2\theta_\alpha+\pi(1+\alpha)}{4}\right)$
b_α	$\frac{1}{4}\cos^2\theta_\alpha$
c_α	$\frac{1}{4}\cos\theta_\alpha\cos^2\left(\frac{2\theta_\alpha+\pi(1+\alpha)}{4}\right)$

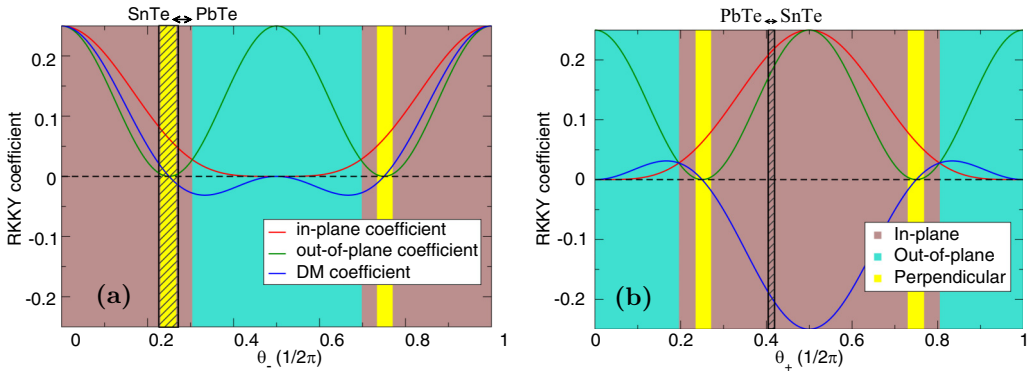

FIG. 2. The evolution of the strength of the RKKY coefficients a_α (in-plane coupling), b_α (out-of-plane coupling), and c_α (Dzyaloshinskii-Moriya coupling) as a function of the spin-mixing parameters θ_α of a topological insulator of the SnTe class. The parameters $\theta_\pm$ reflect the relative strengths of spin-orbit coupling and crystal field in the bulk for the Sn $(-)$ and Te $(+)$ species [with $\theta_\pm = 0$ corresponding to no spin-orbit coupling; see Eq. (7)]. The changing coupling strength of these interaction types results in three qualitatively distinct regions of the RKKY interaction, highlighted by the different background colors: In the brown and in the turquoise regions both spins cant with respect to a ferromagnetic and antiferromagnetic reference state parallel to the x and z axis, respectively, while in the yellow region a collinear coupling parallel to the y axis is preferred (the choice of coordinate system is such that the x axis is aligned with the connection vector of the spin impurities and z points out of plane). The values of $\theta_\pm$ that correspond to the $Pb_xSn_{1-x}Te$ system are indicated by the hatched area.

arguments x , Eq. (24) can be brought to the form

$$\begin{aligned}\frac{E_\alpha^{\rm int}(R_\perp)}{\kappa} &= -\frac{k_F}{2R_\perp^2}\big[\sin(2k_FR_\perp)\big(a_\alpha S_1^xS_2^x + b_\alpha S_1^zS_2^z\big)\\ &\quad - c_\alpha\cos(2k_FR_\perp)\big(S_1^xS_2^z - S_1^zS_2^x\big)\big]\\ &\quad -\frac{1}{8R_\perp^3}\big[\cos(2k_FR_\perp)\big(3a_\alpha S_1^xS_2^x - 2a_\alpha S_1^yS_2^y + 3b_\alpha S_1^zS_2^z\big)\\ &\quad + 3c_\alpha\sin(2k_FR_\perp)\big(S_1^xS_2^z - S_1^zS_2^x\big)\big]. \qquad (29)\end{aligned}$$

In this equation [as well as in the full interaction energy Eq. (24)] the dependence on the coupling vector of the spins is solely through the scalar-valued impurity separation $R_\perp$; this arises from the choice of the coordinate system in which we have rotated the x axis such that it is aligned with the impurity separation vector.

In the lowest order $(1/R_\perp^2)$ there are two Ising-type terms $a_\alpha S_1^xS_2^x + b_\alpha S_1^zS_2^z$ that favor a collinear ferromagnetic (FM) or antiferromagnetic (AFM) coupling, as well as a Dzyaloshinskii-Moriya (DM) term $c_\alpha(S_1^xS_2^z - S_1^zS_2^x)$ that favors the two spins (i) being in the plane formed by the connection vector and the surface normal and (ii) having a relative angle of 90°. Curiously, the collinear terms are $\pi/2$ out of phase with the DM term (a fact also true at order $1/R_\perp^3$); thus, the DM interaction is strongest at the nodes of the FM-AFM Ising-type coupling. However, the most interesting aspect of the interaction energy is that each coupling term is endowed with its own material constant, and as can be seen in Fig. 2 and Table I, these are oscillatory functions of the spin-mixing angles and so of the crystal field and spin-orbit coupling parameters of the bulk. As these prefactors determine the strength of competing terms in the RKKY interaction they will, via the energy minimization of the interaction energy, decisively influence its *qualitative form*. The RKKY interaction in IV-VI topological insulators will therefore be profoundly sensitive to the details of the bulk electronic structure: There is no "universal" form of the RKKY interaction corresponding to, or resulting from, the universality of the Dirac-Weyl operator that describes the topological surface state spectrum.

A striking example of the bulk-boundary connection manifested in the RKKY can be seen from the fact that the material parameters for the group-IV-terminated surface $(-)$ and group-VI-terminated surface $(+)$ are, with a sign change of the DM constant, related to each other by a phase shift of π (see Fig. 2). Thus, when crystal field dominates spin-orbit interaction on the group IV species, i.e., $\theta_- \to 0$, the DM component of the RKKY on the group-IV-terminated surface is maximized; in contradistinction on the group VI termination the opposite is true, and a large DM component is favored by strong spin-orbit coupling. The origin of this difference can be seen in the scattering matrices, Eqs. (22) and (23), for which the off-diagonal (spin-flip) element $\cos^2(\frac{\theta_-}{2})$ is maximized for $\theta_- = 0$. This, in turn, can be traced back to the bulk band edge wave functions (3)–(6), where it is seen that only the Φ_0^- angular momentum ket allows spin flips and that this component of the band edge state is maximum at $\theta_- = 0$. A strong DM interaction is usually associated with substantial spin-orbit coupling; this example highlights the substantial role played by the nontrivial topology of the bulk band structure in the DM interaction.

To investigate the impact of the bulk physics on the impurity spin coupling for a specific example we now consider spin impurities on the tin surface of SnTe and its alloy $Pb_{0.25}Sn_{0.75}Te$, illustrated in Figs. 3(a) and 3(b), respectively. On the tin-terminated surface of SnTe and at an impurity separation of 20 Å both impurity spins couple at FM and parallel to the connection vector. At higher impurity separation the two spins cant away from the connection vector, leading to an increasing out-of-plane component. At an impurity separation of ≈80 Å the canting angle reaches its maximum, and the

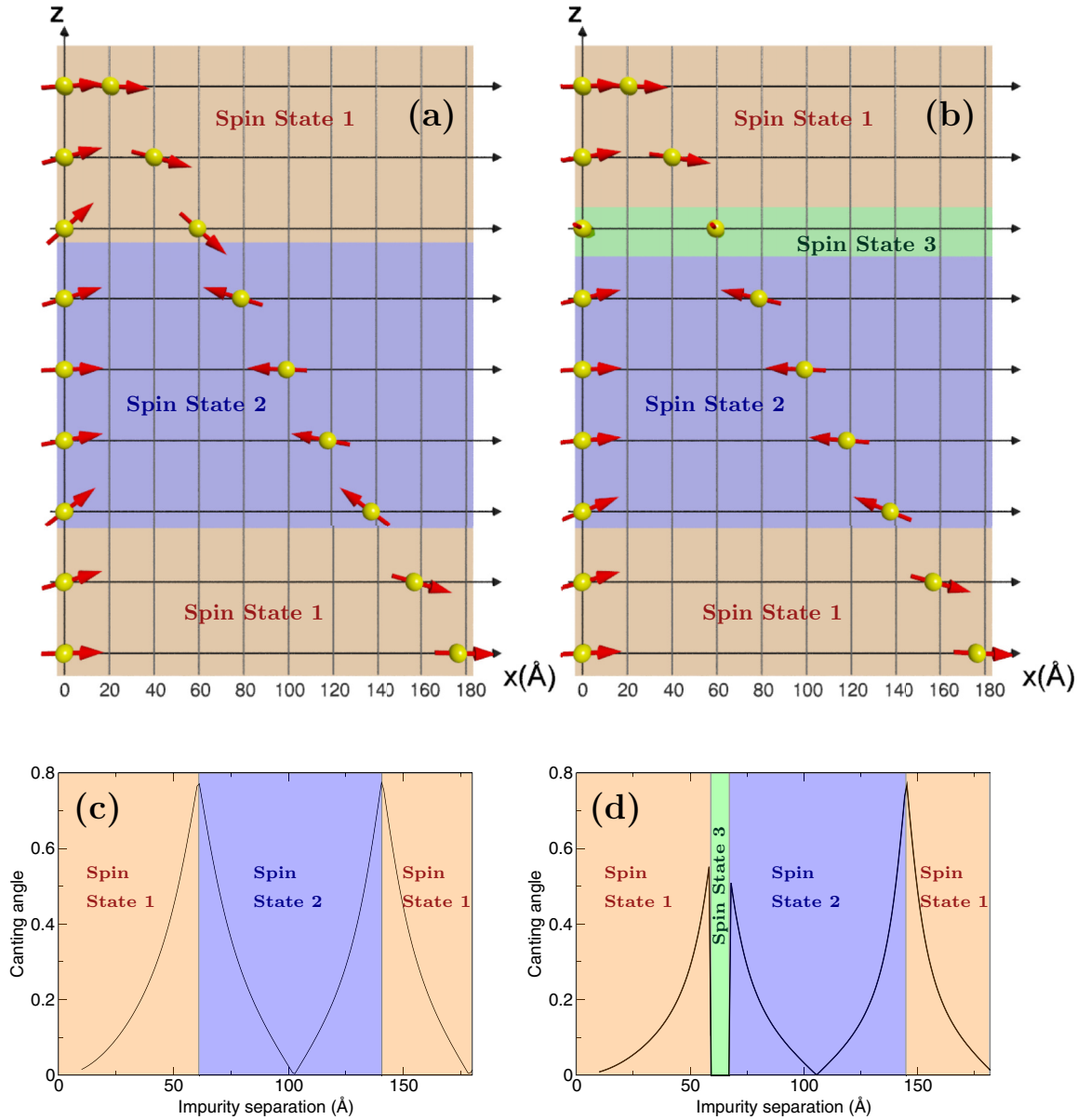

FIG. 3. The RKKY interaction on the tin-terminated (111) surface of (a) and (c) SnTe and (b) and (d) $Pb_{0.25}Sn_{0.75}Te$ at a Fermi energy of 0.1 eV. The SnTe crystal features two distinct spin states: Canting with respect to ferromagnetic or antiferromagnetic coupling parallel to the connection vector of the spins (spin states 1 and 2, respectively). The canting angle is given in (c) and (d). By alloying the SnTe crystal with lead it is possible to open a small window where ferromagnetic coupling perpendicular to the connection vector is preferred (spin state 3). In this state there is almost no noncollinearity of the spins.

configuration flips into an AFM coupling, following which the canting angle then begins to decrease. In the further course of the evolution with increasing separation the two spins oscillate between these two types of spin states with a successively increasing and decreasing canting angle, as shown in Fig. 3(c). The period of oscillation is given by the Fermi energy, which is here set to 0.1 eV. The corresponding behavior on the tin-terminated surface of $Pb_{0.25}Sn_{0.75}Te$ is shown in Fig. 3(b): In large part the interaction resembles that on the surface of SnTe but in a small window from 59 to 67 Å coupling in the direction parallel to the y axis can be observed. As shown in Fig. 3(d), the canting angle is, in that region, rather small, and thus, the coupling can considered to be, as a good approximation, ferromagnetic.

V. DISCUSSION AND CONCLUSIONS

We have employed the RKKY interaction to probe the coupling between the spin structure of the surface state and that of the bulk insulator wave functions in the IV-VI semiconductor crystalline topological insulators. For the (111) surface we have derived the Dirac-Weyl surface state from a fully microscopic description of the bulk insulator, finding in this way an explicit connection between the surface and bulk wave functions. This, in turn, provides a "fully electronic" route from the atomic degrees of freedom of the bulk to the emergent pseudospin structure of the surface state and allows one to probe the impact of bulk physics on the surface RKKY interaction.

We find that the nature of the topological surface state, as probed by the RKKY interaction, is coupled very strongly to the bulk physics: The balance of crystal field and spin-orbit coupling in the bulk insulator determines even the qualitative form of the RKKY interaction. For the group-IV-terminated surface when the crystal field dominates spin orbit in the bulk, the RKKY interaction favors an out-of-plane configuration, while when the reverse is true, an in-plane configuration is favored. On the group-VI-terminated surface the situation is reversed. The equilibrium spin configuration is generally noncollinear, with collinear spins found only when the spin-orbit coupling in the bulk is switched off. In short, while the Dirac-Weyl surface state is "universal" in the sense that the surface state spectrum is always, at low energies, a conical intersection, the surface wave function is not and depends strongly on details of the bulk electronic structure, a fact reflected in the rich dependence of the type of RKKY interaction on the microscopic parameters of the bulk band structure. This essential imprint of the bulk band structure in the topological surface state suggests it would be of interest to apply the formalism presented here to other examinations of the RKKY physics, e.g., going beyond linear order for which additional spin interaction terms appear [32].

[1] S. Saremi, Phys. Rev. B **76**, 184430 (2007).
[2] N. Klier, S. Shallcross, and O. Pankratov, Phys. Rev. B **90**, 245118 (2014).
[3] N. Klier, S. Shallcross, S. Sharma, and O. Pankratov, Phys. Rev. B **92**, 205414 (2015).
[4] N. Klier, S. Sharma, O. Pankratov, and S. Shallcross, Phys. Rev. B **94**, 205436 (2016).
[5] J. Wang, B. Lian, and S.-C. Zhang, Phys. Rev. Lett. **115**, 036805 (2015).
[6] A. A. Zyuzin and D. Loss, Phys. Rev. B **90**, 125443 (2014).
[7] W. Qin and Z. Zhang, Phys. Rev. Lett. **113**, 266806 (2014).
[8] V. I. Litvinov, Phys. Rev. B **89**, 235316 (2014).
[9] D. K. Efimkin and V. Galitski, Phys. Rev. B **89**, 115431 (2014).
[10] V. Cheianov, M. Szyniszewski, E. Burovski, Y. Sherkunov, and V. Fal'ko, Phys. Rev. B **86**, 054424 (2012).
[11] Z. L. Li, J. H. Yang, G. H. Chen, M.-H. Whangbo, H. J. Xiang, and X. G. Gong, Phys. Rev. B **85**, 054426 (2012).
[12] D. A. Abanin and D. A. Pesin, Phys. Rev. Lett. **106**, 136802 (2011).
[13] J.-J. Zhu, D.-X. Yao, S.-C. Zhang, and K. Chang, Phys. Rev. Lett. **106**, 097201 (2011).
[14] Q. Liu and T. Ma, Phys. Rev. B **80**, 115216 (2009).
[15] H.-R. Chang, J. Zhou, S.-X. Wang, W.-Y. Shan, and D. Xiao, Phys. Rev. B **92**, 241103(R) (2015).
[16] M. V. Hosseini and M. Askari, Phys. Rev. B **92**, 224435 (2015).
[17] B. A. Volkov and O. A. Pankratov, J. Exp. Theor. Phys. **48**, 687 (1978).
[18] B. A. Volkov, O. A. Pankratov, and A. V. Sazonov, J. Exp. Theor. Phys. **58**, 809 (1983).
[19] B. A. Volkov and O. A. Pankratov, JETP Lett. **42**, 178 (1985).
[20] O. A. Pankratov, S. V. Pakhomov, and B. A. Volkov, Solid State Commun. **61**, 93 (1987).
[21] S. Safaei, P. Kacman, and R. Buczko, Phys. Rev. B **88**, 045305 (2013).
[22] Y. Tanaka, Z. Ren, T. Sato, K. Nakayama, S. Souma, T. Takahashi, K. Segawa, and Y. Ando, Nat. Phys. **8**, 800 (2012).
[23] Y. Tanaka, T. Shoman, K. Nakayama, S. Souma, T. Sato, T. Takahashi, M. Novak, K. Segawa, and Y. Ando, Phys. Rev. B **88**, 235126 (2013).
[24] Y. Tanaka, T. Sato, K. Nakayama, S. Souma, T. Takahashi, Z. Ren, M. Novak, K. Segawa, and Y. Ando, Phys. Rev. B **87**, 155105 (2013).
[25] P. Barone, T. Rauch, D. Di Sante, J. Henk, I. Mertig, and S. Picozzi, Phys. Rev. B **88**, 045207 (2013).
[26] M. Drüppel, P. Krüger, and M. Rohlfing, Phys. Rev. B **90**, 155312 (2014).
[27] Y. Shi, M. Wu, F. Zhang, and J. Feng, Phys. Rev. B **90**, 235114 (2014).
[28] C. M. Polley, P. Dziawa, A. Reszka, A. Szczerbakow, R. Minikayev, J. Z. Domagala, S. Safaei, P. Kacman, R. Buczko, J. Adell *et al.*, Phys. Rev. B **89**, 075317 (2014).
[29] O. A. Pankratov, Semicond. Sci. Technol. **5**, S204 (1990).
[30] A. A. Taskin, F. Yang, S. Sasaki, K. Segawa, and Y. Ando, Phys. Rev. B **89**, 121302(R) (2014).
[31] O. V. Yazyev, J. E. Moore, and S. G. Louie, Phys. Rev. Lett. **105**, 266806 (2010).
[32] M. Shiranzaei, J. Fransson, H. Cheraghchi, and F. Parhizgar, Phys. Rev. B **97**, 180402(R) (2018).